Effects of Aerosols on the Radiative Properties of Clouds

JONATHAN P. TAYLOR AND MARTIN D. GLEW

Meteorological Research Flight, The Met. Office, Farnborough, Hampshire, United Kingdom

JAMES A. COAKLEY JR. AND WILLIAM R. TAHNK

College of Oceanic and Atmospheric Sciences, Oregon State University, Corvallis, Oregon

STEVEN PLATNICK

NASA Goddard Space Flight Center, Greenbelt, Maryland

PETER V. HOBBS AND RONALD J. FEREK*

Atmospheric Sciences Department, University of Washington, Seattle, Washington

(Manuscript received 9 July 1996, in final form 20 March 1997)

ABSTRACT

The influence of anthropogenic aerosols, in the form of ship exhaust effluent, on the microphysics and radiative properties of marine stratocumulus is studied using data gathered from the U.K. Met. Office C-130 and the University of Washington C-131A aircraft during the Monterey Area Ship Track (MAST) experiment in 1994. During the period of MAST, stratocumulus clouds were studied during 11 flights and a wide range of levels of background pollution was observed. The impact of the aerosol emitted from the ships was found to be very dependent on the background cloud microphysical conditions. In clouds of continental influence, the susceptibility of the cloud to further aerosol emissions was low, with a correspondingly weak microphysics and radiation signature in the ship tracks. In clean clouds, changes in droplet concentration of a factor of 2, and reductions in droplet size of up to 50%, were measured. These changes in the microphysics had significant impacts on the cloud radiative forcing. Furthermore, as a result of the cloud droplet size being reduced, in some cases the drizzle was suppressed in the clean clouds, resulting in an increase in liquid water path in the polluted ship track environment. The impact of this combined change in liquid water path and droplet radius was to increase the cloud radiative forcing by up to a factor of 4.

1. Introduction

The radiative properties of a cloud in its liquid phase are largely determined by the droplet sizes in the cloud and the column liquid water path (Slingo and Schrecker 1982). The droplet size is determined by the droplet concentration and the available liquid water. In turn, the droplet concentration is determined primarily by the concentration of cloud condensation nuclei (CCN) in the air (Twomey 1974). Twomey (1977) discussed the impact of changes in droplet concentration on cloud albedo and showed that albedo is increased when the droplet concentration is increased if the liquid water path remains constant.

Squires and Twomey (1960) found that droplet concentrations are different in maritime and continental clouds. CCN concentrations can be modified by anthropogenic emissions of aerosols (Braham 1974; Hobbs et al. 1970, 1974; Eagan et al. 1974). Hence, given the cloud–aerosol feedbacks discussed above, anthropogenic pollution has the potential to modify climate (Charlson et al. 1992; Hobbs 1993).

The effect of aerosol acting to reduce the droplet size within clouds was first postulated by Twomey (1974). This decrease in droplet size would act to increase cloud albedo and hence possibly cool the climate system. Later Twomey et al. (1984) estimated that this cooling might be sufficient to offset partially the greenhouse warming resulting from increased greenhouse gas concentrations. Charlson et al. (1992) considered this effect for sulphate aerosols. More recently Jones and Slingo (1996) have used a general circulation model (GCM) to estimate the

* Current affiliation: Office of Naval Research, Washington, D.C.

Corresponding author address: Dr. Jonathan P. Taylor, Remote Sensing Branch, The Met. Office, Farnborough, Hampshire GU14 0LX, United Kingdom.
E-mail: jptaylor@meto.gov.uk

indirect radiative forcing by anthropogenic sulphate aerosols since the beginning of the industrial era. Jones and Slingo use a range of parameterisations relating aerosol concentration to droplet size and run the GCM to study the resulting changes in the top-of-atmosphere net radiation.

The ''ship track'' phenomenon offers a potential test of the relationships between aerosol emissions and the radiative properties of warm clouds. In this paper the term ''ship plume'' will be used to describe the aerosol plume emanating from a ship, and the term ''ship track'' will be used to describe changes in the cloud microphysics produced by a ship plume.

Ship tracks were first observed in otherwise clear skies (Conover 1966). More commonly ship tracks have been observed in satellite imagery as bright linear features in stratocumulus cloud fields (Coakley et al. 1987). Radke et al. (1989) have presented in situ measurements of ship tracks observed during the First International Satellite Cloud Climatology Project (ISCCP) Regional Experiment (FIRE 87). Radke et al. showed that the droplet size in the ship track decreased significantly and that the liquid water content in the ship track was locally higher than in the background. Albrecht (1989) later postulated that this increase in liquid water content was attributable to drizzle suppression in the track because of the smaller droplet sizes reducing the coalescence efficiency. In situ measurements in two ship tracks off the Washington coast (Ferek et al. 1998) also showed reduction in the amount of drizzle-sized drops in the track, but no corresponding increase in liquid water content was observed.

During June 1994 the U.K. Met. Office Meteorological Research Flight (MRF) C-130, the University of Washington's (UW's) C-131A, the National Aeronautics and Space Administration's ER-2 high-altitude aircraft, the Naval Research Laboratory airship, and a research vessel the R/V *Glorita* took part in the Monterey Area Ship Track (MAST) experiment (Durkee et al. 2000). During this experiment the effluents from dedicated navy vessels and commercial ships of opportunity were studied to determine the effects of aerosol emissions on marine stratocumulus. The in situ data presented in this paper come from the MRF C-130 and the UW C-131A, which together flew 17 flights to study the effluents from 26 different ships. The data gathered included both aerosol and cloud microphysics and radiometric measurements.

In this study the data gathered during the MAST experiment will be used to study the impact of anthropogenic aerosols on marine boundary layer clouds. In particular the issue of modification of cloud liquid water path resulting from a reduction in droplet size leading to a cutting off the drizzle process will be analyzed. This process has the potential to increase the radiative impact of aerosols on the cloud layer beyond just changes in drop size. Current GCM simulations of the radiative forcing due to reductions in cloud droplet size do not deal with these effects, and this omission is discussed.

In section 2 a brief description of the key instrumentation used during MAST is discussed. Section 3 attempts to put the measurements gathered during MAST into context with other similar datasets of stratocumulus properties. In section 4 the concept of cloud susceptibility is discussed, and the use of this quantity as an indicator of the sensitivity of clouds to modification in droplet concentrations is evaluated. Section 5 uses the aircraft radiation measurements to characterize the radiative signature of the ship tracks and compares the results with recent GCM predictions.

2. Aircraft instrumentation

The MRF C-130

The MRF, a part of The Met. Office, operates a Royal Air Force C-130 Hercules aircraft that has been modified extensively to make it suited to a wide range of atmospheric research work.

A brief description of some of the instruments is given here. A more complete description of the standard meteorological instrumentation is given by Rogers et al. (1995), of the cloud physics instrumentation by Martin et al. (1994) and Brown (1993), and the radiation instrumentation by Kilsby et al. (1992) and Saunders et al. (1992).

1) RADIATION INSTRUMENTATION

Broadband hemispherical irradiances are measured with Eppley pyranometers, two on the top of the aircraft and two on the underside. Each pair consists of one instrument fitted with a clear dome (Schott filter WG295, passband approximately 0.3–3.0 μm) and another fitted with a red dome (Schott filter WG715, passband approximately 0.7–3.0 μm). The red-dome filter separates the near-infrared part of the solar spectrum, where absorption by water vapor and condensed water are important, from the visible part, where molecular scattering is significant. The visible irradiance can therefore be computed by differencing the clear-dome and red-dome measurements.

Under conditions of predominantly direct irradiance the upper instruments have to be corrected for deviations from the local horizontal and a non-ideal cosine response. A thorough description of the techniques used is given by Saunders et al. (1992), whose results suggested that diffuse irradiances were the most accurate measurements, approaching 2%. For clear-sky downwelling irradiances the leveling and noncosine corrections act to increase the uncertainty in the measurements to approximately 3%.

The Microwave Airborne Radiometer Scanning System (MARSS) is flown on the C-130. The MARSS is fully described by Jones (1991) and English et al.

(1994). The MARSS measures emission at 89 and 157 GHz and can be used to retrieve cloud liquid water path (English 1995).

The Multi-Channel Radiometer (MCR) (Rawlins and Foot 1990) measures radiances in 14 narrow spectral bands between 0.55 and 12 μm. The MCR is mounted in a pod on the port wing of the aircraft and can view in the zenith and nadir and at angles out to 60° from the nadir. Internal calibration targets can also be viewed for calibration of the thermal infrared channels. The field of view of the optical system is 1.5°. The incident radiation is split into four streams, two thermal and two solar, and viewed by four detectors. Each detector has a rotating filter wheel with four filters. One complete revolution of a filter wheel takes 4 s.

Cloud optical depth, τ, and cloud droplet effective radius, r_e, can be retrieved using measurements of the reflectance at two wavelengths in the visible or near-infrared. The reflectivity in a spectral region of weak liquid water absorption (e.g., 0.55 or 1.25 μm) is relatively insensitive to changes in r_e but monotonically increases with increasing τ; this allows a retrieval of τ by reference to a lookup table of model reflectances for varying clouds. This retrieved τ can then be combined with the reflectance at a wavelength of strong liquid water absorption (e.g., 2.01 or 2.26 μm) to retrieve r_e. A thorough description of the scheme is given by Rawlins and Foot (1990), and an improvement to the scheme is given by Taylor (1992).

2) Aerosol and cloud physics instrumentation

Liquid water content is measured on the C-130 using a Johnson–Williams hot-wire probe. This instrument is insensitive to droplets larger than about 30-μm radius, and its accuracy is $\pm 10\%$.

The cloud particle size distribution is measured by a Particle Measuring Systems (PMS) Forward Scattering Spectrometer Probe (FSSP). Particles are assumed to be perfectly spherical and composed of pure water. Measurements of the rate of sizing events and the true airspeed allow inference of droplet number densities. The instrument records the number of droplets detected in 15 size categories in one of four ranges of droplet diameters selected by the operator: 2–47, 2–32, 1–16, or 0.5–8 μm. The FSSP has some major limitations. Specifically, the sample volume particle rejection criteria are not defined with sufficient accuracy to enable integrated quantities such as liquid water content to be obtained with any great accuracy directly from the spectra. In this work the liquid water contents are taken from measurements by the Johnson–Williams probe. The effective radius is taken from FSSP measurements, and we therefore assume that the FSSP measures the spectral shape accurately, although the absolute concentration may be in error.

The FSSP is calibrated by sampling glass beads of known sizes, allowances being made for the difference in refractive index of glass to that of water. The accuracy of the FSSP sizing is, at best, ± 1-μm radius.

The droplet spectra are used to compute the cloud droplet effective radius defined as

$$r_e = \frac{\int n(r) r^3 \, dr}{\int n(r) r^2 \, dr}, \tag{1}$$

where r is the droplet radius and $n(r)$ the concentration of droplets of radius between r and $r + dr$.

Larger water droplets are measured using a PMS 2-DC probe. This instrument images particles in the range 25–800-μm diameter. In the 2-DC probe an array of photodiodes is illuminated by a He–Ne laser. A particle in the airflow will cross the laser beam and cast a shadow on the photodiodes. These images can be sized and counted to produce a spectrum. Combining the spectra from the FSSP and 2-DC instruments to give an r_e therefore includes the contribution due to the larger drizzle-sized droplets.

Aerosol concentration is measured by a PMS Passive Cavity Aerosol Spectrometer Probe (PCASP). This instrument counts and sizes aeresol in 15 size intervals covering the size range 0.1–3.0-μm diameter. Heaters in the tip of the inlet pipe to the PCASP and the sheath of dry air used to ''focus'' the sample into the path of the laser beam will both act to dry the aerosol. However, if the aerosol is particularly moist, or indeed saturated within cloud, then spurious results can be obtained. Also shattering of water droplets on the probe inlet can cause anomalously large concentrations to be recorded. For these reasons measurements made by the PCASP are used only outside of clouds.

A description of the extensive instrumentation aboard the UW C-131A aircraft has been given by Hobbs et al. (1991) and elsewhere in this special issue (e.g., Hobbs et al. 2000; Ferek et al. 2000).

3. Stratocumulus variability

It is useful to be able to put the measurements made during MAST in context with those observed in stratocumulus around the world. Figure 1 shows histograms of the background stratocumulus cloud effective radius at cloud top during profiles and straight and level runs for several regions of the world measured by the FSSP. All of these observations were made with the U.K. C-130 between 1987 and 1995. As can be seen there is a tendency toward larger effective radii in the more remote regions, away from anthropogenic pollution sources, with the largest average effective radii being observed in the South Atlantic. The histograms of effective radius for FIRE 87 and MAST (Fig. 1c), both experiments that took place off the Californian coast,

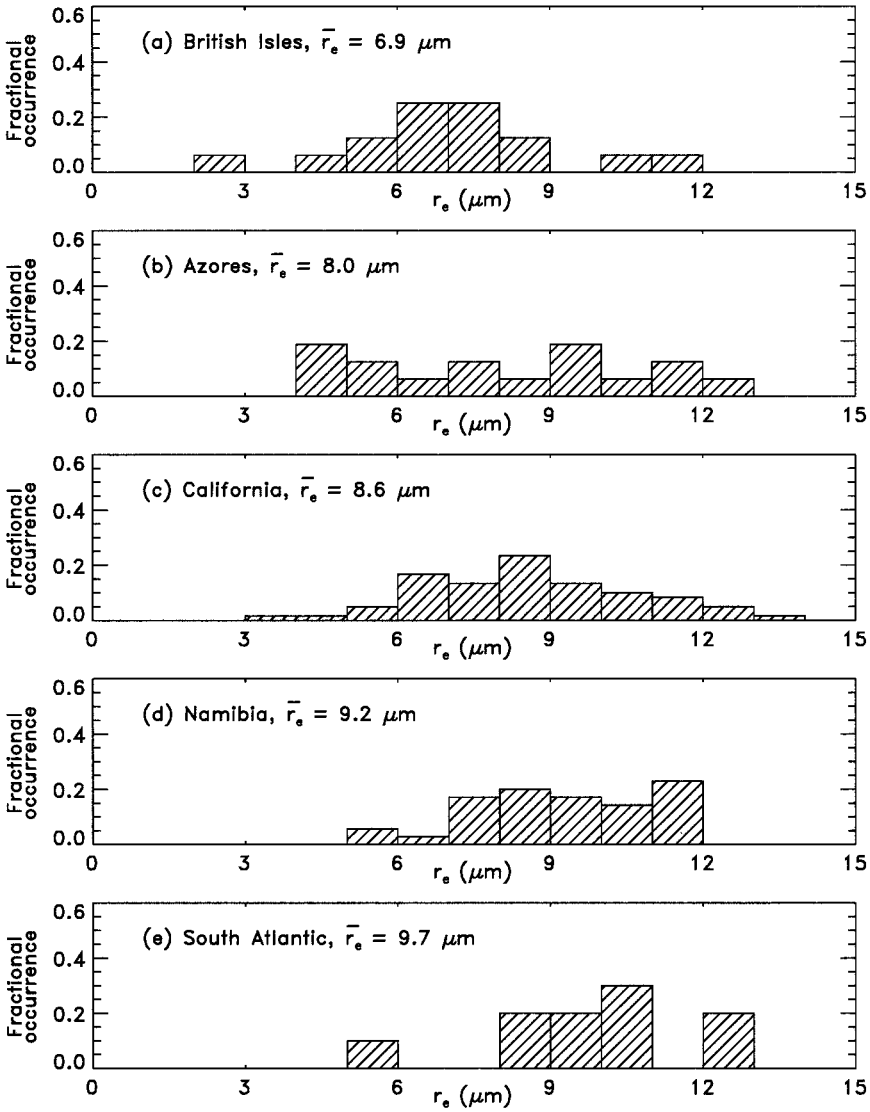

FIG. 1. Histograms of the fractional occurrence of cloud-top effective radius at various locations around the world as measured by the C-130.

show that in this region a wide range of conditions can occur since the effective radius ranges from 3 to 14 μm. Han et al. (1994) carried out a near-global survey of effective radius based on ISCCP data. The range of r_e observed by Han et al. is consistent with the values presented in Fig. 1.

Data from 30 passes through ship tracks have been used to look at the properties of the background unpolluted clouds and the modified ship track clouds during MAST. These data were collected by visual inspection of time series of each run near cloud top and above cloud that passed perpendicular to a ship track and selecting time periods within the track and either side of it. The track was identified both by inspection of the data and by coincidence with the expected position of the track as estimated by the navigator using a knowledge of the ship's speed, heading, and surface winds. The data associated with the ship track were averaged over the entire width of the ship track, which varied from around 1 to 12 km. The background cloud statistics were gathered from the data either side of the track at a distance at least several hundred meters away from the influence of the track. The length of the data time series used in the background statistics was typically around 30 km.

The effective radius of the cloud droplet distribution can be computed to cover two spectral ranges: that covered only by the FSSP and that covered by the combined FSSP and 2-DC instruments. Figure 2 shows, in the upper panel, the change in effective radius observed over the FSSP spectral interval in the ship track as a function of the background cloud droplet concentration.

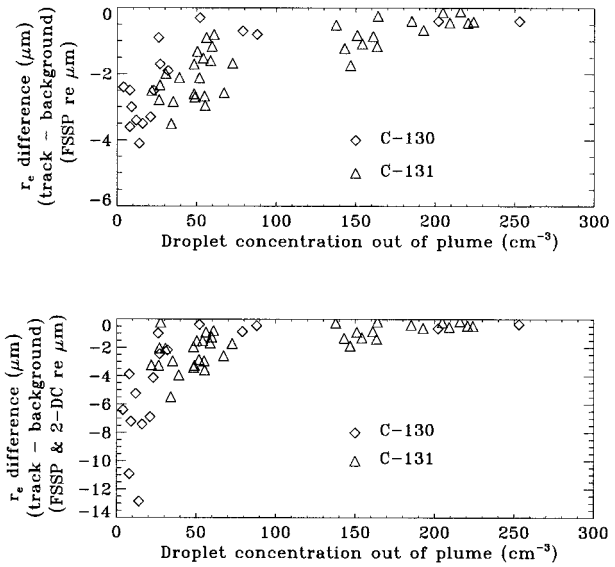

FIG. 2. Difference in cloud droplet effective radius between ship track and background cloud as a function of background droplet concentration, averaged over all in-track and background data. (upper panel) FSSP spectra only, (lower panel) combined FSSP and 2-DC spectra.

The lower panel shows the same plot except the spectra of the 2-DC and FSSP are combined. The droplet concentrations plotted are those measured by the FSSP only. This does not lead to any significant error since droplet concentrations measured by the 2-DC probe are very much lower than those measured by the FSSP (typically 2-DC droplet concentrations are less than 1 cm^{-3}). Data from the MRF C-130 are shown as diamonds and those from the UW C-131A are shown as triangles. It should be noted that due to differences in the 2-DC probes on the two aircraft, and the different techniques used to process the 2-DC imagery by the UW and MRF, the absolute concentrations of drizzle-sized drops were in poor agreement. It is possible that as a result of these differences there might be some, as yet undetermined, differences in r_e between the two probes.

These two scatterplots clearly show that the changes in effective radius are largest where the ship track has formed in clouds with a low background droplet concentration. This is consistent with our understanding of the relationship between CCN and effective radius. In the clouds with higher droplet concentrations, the addition of extra aerosol from the ship stack fails to generate many more droplets than were already observed, and hence the change in droplet size is small. The lower panel of Fig. 2 also shows the important contribution to the cloud effective radius in the large drizzle size region of the spectra as measured by the 2-DC. This is particularly important in the clouds with low background droplet concentrations where we might expect drizzle to occur. Despite the differences in the two 2-DC probes, mentioned above, the MRF C-130 and UW C-131A data both show the same pattern with the largest differences in r_e occurring in the cleanest air masses.

4. Cloud susceptibility

It is useful to be able to describe how sensitive a particular cloud is likely to be to changes in the droplet concentration that may occur as a result of increased aerosol concentration in the boundary layer. Platnick and Twomey (1994) used the rate of change of cloud albedo with droplet concentration, termed the cloud susceptibility, as an indicator of the sensitivity of a cloud to changes in droplet concentration. In this work the form of susceptibility described by Taylor and McHaffie (1994) is used. This formulation of cloud susceptibility differs from that described in Platnick and Twomey by the inclusion of a term k that relates the mean volume radius of a droplet spectrum to the effective radius of the spectrum:

$$r_v^3 = kr_e^3. \tag{2}$$

It should be noted that the susceptibility could be computed using the mean volume radius, but in this work the effective radius is chosen, as it is this description of the droplet spectrum that is used most widely in the literature and in numerous radiation schemes (e.g., Slingo and Schrecker 1982).

Following Taylor and McHaffie (1994), the susceptibility is calculated under the conditions of constant liquid water using the expression

$$\frac{dA}{dN} = \frac{4\pi\rho_l}{9L}A(1 - A)kr_e^3 \tag{3}$$

from measurements of L the liquid water content (g m^{-3}), A the albedo, r_e the cloud droplet effective radius (m), and N the cloud droplet concentration (m^{-3}); ρ_l is the density of liquid water (g m^{-3}). Here, L and r_e are measured from a straight and level run near cloud top, and A is measured from a run above cloud vertically stacked above the in-cloud measurement run. It should be noted that in the derivation of Eq. (3), described fully in Platnick and Twomey (1994) and Taylor and McHaffie (1994), the albedo, A, refers to the visible albedo (0.3–0.7 μm). The visible albedo is measured by differencing measurements taken with clear-dome (0.3–3.0 μm) and red-dome (0.7–3.0 μm) pyranometers mounted on the top and bottom of the aircraft. The UW C-131 aircraft did not fly red-domed instruments, and hence the susceptibility could not be computed. Susceptibility measurements and computations are therefore presented using data measured only by the MRF C-130.

Platnick and Twomey (1994) presented a form of the susceptibility equation that allows for a change in cloud liquid water path with changes in droplet concentration. They used the relation $L = \alpha N^{\beta}$. This functional relationship between L and N resulted in an extra multiplying term $(1 + 2\beta)$ on the right-hand side of Eq. (3), such that when L remains constant (i.e., $\beta = 0$) Eq. (3)

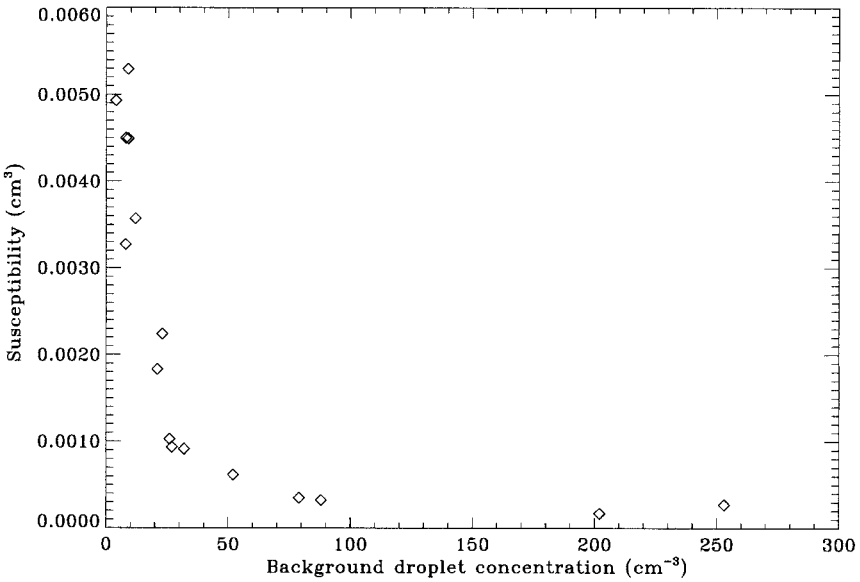

FIG. 3. Cloud susceptibility as a function of measured background droplet concentration.

is obtained. This form of the susceptibility equation is not used here since our observations suggest that this relationship between L and N is not very robust. It is noted, however, that changes in liquid water path often occur as a result of increases in droplet concentration and that this is a limitation in the use of cloud susceptibility in this form. The importance of changes in liquid water content will be returned to in section 5.

The value of k has been determined for each case depending on the background droplet concentration; $k = 0.80$ in maritime air masses ($0 < N < 185$ cm^{-3}) and $k = 0.67$ in continental air masses ($N > 185$ cm^{-3}) as described by Martin et al. (1994). The term k is explicitly related to the chemistry and spectra of the cloud condensation nuclei that are activated to form the cloud droplets. In reality there will not be a sudden change in k as used in this study and in the parameterization of Martin et al. More realistically there will be a gradual change in the relationship between the mean volume radius and the effective radius. In particular, for the case of a ship track where the new CCN available in the ship exhaust plume are likely to be of a totally different chemistry than those in the background clouds, there will probably be a gradual change of k with the age of the ship track. Such changes of k are not accounted for in this work but are considered to be small compared to the other changes in the cloud microphysics that have been observed to occur in the ship track environment.

In the results presented here, L is measured using a Johnson–Williams hot-wire probe. The r_e can be measured either using the FSSP or by combining the spectra of the FSSP and the PMS 2-DC, as described earlier. As the computation of susceptibility requires albedo measurements from a run vertically stacked above the in-cloud run, the number of available ship track transects available for study is reduced to 16 that come from six different flights.

Figure 3 shows the susceptibility of the background clouds measured during MAST, computed from the FSSP droplet spectra, as a function of the background cloud droplet concentration. As can be seen the susceptibility decreases rapidly with increasing droplet concentration, indicating that clouds in continental air masses will show little sensitivity to further increases in droplet concentration. For the 16 cases where we have computed the background susceptibility we also have available the microphysical properties of the polluted ship track cloud. This dataset is therefore potentially very useful for studying how susceptibility can be used as a predictor of changes in the radiative properties of a cloud. The droplet concentration in the background cloud and in the ship track has to be computed since the liquid water content and r_e are measured by different instruments. The assumption here is that the Johnson–Williams probe measures the liquid water content accurately and that the FSSP measures the droplet spectral shape accurately. The droplet concentration is computed by maintaining balance in the relationship

$$L = \frac{4}{3}\pi\rho_l k r_e^3 N. \tag{4}$$

In this study the cloud droplet concentration has been incremented by 1-cm^{-3} intervals from the background value to that measured in the ship track in a finite-difference manner. On each increment the cloud droplet effective radius is recomputed, assuming conservation of liquid water, and a new cloud albedo is computed using the previous value of cloud susceptibility. This

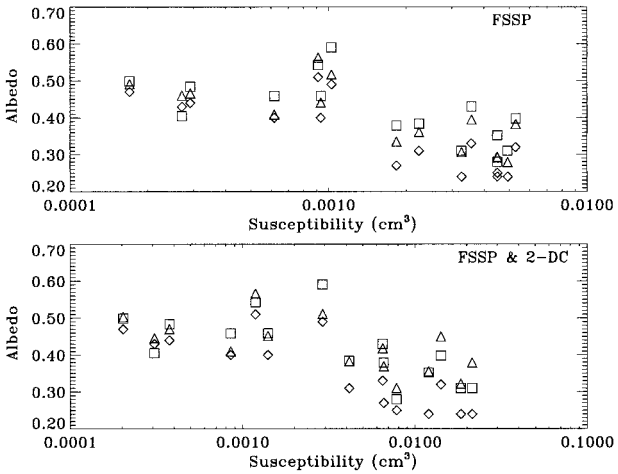

FIG. 4. The background cloud susceptibility has been used to predict the change of albedo over the ship track. The observed background albedo is shown as diamonds, the predicted change in albedo as triangles, and the actual observed change in albedo as squares. The albedos are plotted as a function of cloud susceptibility. The upper panel shows the results using the FSSP spectra to compute the r_e; the lower panel shows results using the combined FSSP and 2-DC spectra.

new albedo is then combined with the new effective radius to compute a new susceptibility and the process is continued. In this manner, the final albedo of the ship track can be predicted and compared with the actual albedo measured by the aircraft above the ship track.

Figure 4 shows the albedo plotted as a function of the background cloud susceptibility. The effective radius is computed for the susceptibility calculations using the FSSP spectra alone in the upper panel and with the combined spectra of the FSSP and 2-DC probes in the lower panel. The background albedos are shown as diamonds, the predicted values for the ship track as triangles, and the observed values in the ship track as squares. For the clouds of low background susceptibility, the background albedo is higher than that for the clouds of high susceptibility and there is little predicted or observed change in cloud albedo over the ship tracks. As the susceptibility of the background cloud increases, the predicted changes in albedo increase. The runs above cloud to measure the actual albedo were carried out either immediately before or after the in-cloud run where the drop size measurements were made. The two runs were flown so as to correct for drift of the cloud during the time period of the runs. In this manner differences between the predicted and observed albedo changes due to the background variability of the cloud field were hopefully minimized. It is accepted, however, that some effects due to inhomogeneities may persist.

For the results using only the FSSP spectra (upper panel in Fig. 4) the predicted albedos are predominantly lower than those actually observed over the ship track. When the combined spectra are used (lower panel in Fig. 4) the agreement is generally better; on some occasions the observed albedo is lower than that predicted and on other occasions the converse is true.

Figure 4 clearly shows that susceptibility can be used as a rough predictor of the sensitivity of a cloud to a polluting episode. There are, however, obvious difficulties in predicting the absolute magnitude of the changes that will occur. The formulation of the equation for cloud susceptibility has, in its definition, assumed that the liquid water content of the cloud remains constant. The major precipitation process in stratocumulus is autoconversion, the collision of small droplets with one another; the efficiency of this process is partly determined by the range of sizes of the droplets within the cloud and their concentration. As droplet concentrations increase, the sizes of the drops within a cloud decrease, and these factors will act to decrease the efficiency of the coalescence process and reduce the precipitation rate. Therefore, in the ship track environment, if the ship plume aerosol is injected into a stratocumulus cloud sheet that is experiencing drizzle episodes, the increased droplet concentration could act to suppress the drizzle. As a result the localized liquid water path within the plume could be higher than in the background cloud by virtue of the reduced loss of liquid water through drizzle processes. Such a hypothesis was presented by Radke et al. (1989) and is the subject of a paper in this issue, Ferek et al. (2000). Pincus and Baker (1994) highlighted the impact of drizzle processes and also changes in cloud thickness that act to affect the cloud susceptibility. These processes, and others, which may act to change the physical and microphysical structure of the cloud following a pollution episode, are not accounted for in the simple model of cloud susceptibility presented here and may account for the differences between the observed and predicted changes. In addition inhomogeneities of the cloud field and changes in the cloud between the in-cloud run and the above-cloud run may contribute to the discrepancies observed. There is strong evidence of changes in liquid water path in some of the ship tracks observed during MAST by the U.K. C-130; this evidence and the effects of these changes on the radiative properties of the polluted cloud are of importance.

It should be noted that although susceptibility, as described here with constant liquid water content, cannot be used to predict accurately the absolute magnitude of the changes in the radiative properties of the polluted cloud layer, it can be used to give an estimate of the changes and a clear indication of which clouds are likely to be affected the most and, in this respect, is a useful indicator of the importance of various cloud sheets in climate modulation in a future, possibly more polluted, atmosphere. This issue is dealt with in more detail by Platnick et al. (2000) where a modified version of the susceptibility parameter is introduced.

5. The indirect radiative forcing of aerosols

Ship tracks are not expected to have any impact on climate, or even on the top-of-atmosphere irradiances,

because of their limited spatial extent. However, they do provide measurable examples of albedo modification that can aid understanding of the impact of aerosols on cloud radiative properties. In common with the work of Jones and Slingo (1996), we will present results of top-of-atmosphere radiative forcing, R, in this case due to ship tracks, as a change in the top-of-atmosphere net forcing; thus,

$$R = (\mathrm{SW}_{\mathrm{tr}} - \mathrm{SW}_{\mathrm{bck}}) + (\mathrm{LW}_{\mathrm{tr}} - \mathrm{LW}_{\mathrm{bck}}), \quad (5)$$

where SW is the net top-of-atmosphere shortwave irradiance; LW the net top-of-atmosphere longwave irradiance (where downward is positive); and the subscripts ''tr'' and ''bck'' refer to the ship track and background clouds, respectively.

It is difficult to produce a realistic model of a cloud from in situ measurements, since often the vertical resolution of the observations is insufficient. This is particularly the case for stratocumulus clouds that are drizzling, since the vertical structure of the distribution of liquid water and droplet size may not increase linearly with height as they do in nonprecipitating stratocumulus. In fact, the drizzle may redistribute the liquid water such that the maxima is no longer at the cloud top. For this reason we have used remote sensing techniques to study the radiative properties of the ship tracks.

Results from four ship track transects, from three flights, will be presented where a signature was observed in the radiation measurements during runs above cloud crossing the line of the ship track. The thickness of the cloud is determined from an aircraft profile, and the cloud is modeled as a single-layer cloud with fixed effective radius and liquid water content such that the integrated liquid water path matches that retrieved by the remote sensing instruments. The effective radius retrieval was carried out using simultaneous measurements of near-infrared reflectances (Rawlins and Foot 1990; Taylor 1992, 1994). For one of the flights the cloud liquid water path was retrieved from microwave emission measurements from the cloud field; for the other two cases the cloud is modeled in the same way, but due to instrumental problems with the microwave radiometer, the liquid water path (LWP) of the clouds is determined by combining the optical depth τ and effective radius r_e retrieved from near-infrared reflectances using the relation

$$\mathrm{LWP} = \frac{2\tau r_e \rho_l}{3}. \quad (6)$$

This technique is described by Taylor and English (1995), who showed that such a model of a stratocumulus cloud field gave good agreement with a more detailed multilevel model. For one of the four cases both the microwave radiometer and near-infrared reflectances were available, allowing a direct comparison of these two techniques. In this case the background cloud LWP was measured as 124.7 and 130.5 g m^{-2}, while in the ship track the LWPs were 188.8 and 177.6 g m^{-2}, using the microwave radiometer and near-infrared reflectances, respectively. As these two sets of measurements were in good agreement, only the microwave radiometer values were used in the subsequent study.

Profiles of temperature and humidity through the cloud layer and the lower troposphere were obtained from aircraft measurements, and these were supplemented by a midlatitude summer model for higher levels (McClatchey et al. 1972). Ozone is also taken from the corresponding McClatchey profile. The volume mixing ratio of oxygen is taken as 0.209 46, following the value given in Goody and Yung (1989). The mixing ratio of carbon dioxide is taken as 355 ppmv (Houghton et al. 1990). These profiles were input to the radiation code of Edwards and Slingo (1996), which can be used to model irradiances over both the longwave and shortwave regions of the spectrum. In this study the longwave calculations were carried out using nine bands covering the spectral range 0–3000 cm^{-1}; the shortwave calculations were carried out using the 220-band version of the code that covers the spectral range 0.2–10 μm. The shortwave version of this code has been validated against aircraft measurements of irradiances (Taylor et al. 1996), and good agreement to within 3% was found under clear-sky conditions. For each of the three cases the Edwards Slingo code has been run using the solar constant for 8 June 1994, and the diurnal average of the top-of-atmosphere forcing has been computed at a position of 36.5°N, 122°W, which is just off the California coast near Monterey, California, the operating area for MAST.

Previous modeling estimates of the indirect cloud forcing of aerosols (Jones and Slingo 1996) have considered only what we term ''forcing of the first kind,'' namely, the radiative effects of the cloud arising from the impact of aerosol on the droplet radius. Here we shall also consider indirect ''forcing of the second kind,'' namely, the radiative effects resulting from the impact of increased aerosol concentrations both on the droplet radius and on the liquid water path through actions such as drizzle suppression. In the radiation modeling presented here the forcing due to the combined effects of LWP and r_e changes has been studied, shown as solid lines in Fig. 5, and the effects of changes to the droplet size only are shown as dashed lines.

In the simulations where the liquid water path was fixed, the droplet size changes were modeled by using the FSSP droplet spectra measured during a run near cloud top to compute the effective radius. The liquid water content was fixed such that when integrated across the cloud thickness the LWP was equal to that retrieved by remote sensing techniques in the ship track. In computing the cloud properties for these simulations the assumption is that the liquid water that would have been in the drizzle-size droplets in the background cloud is evenly distributed across the FSSP size spectra but the droplet spectral shape is maintained.

In the other simulations, where r_e and LWP are al-

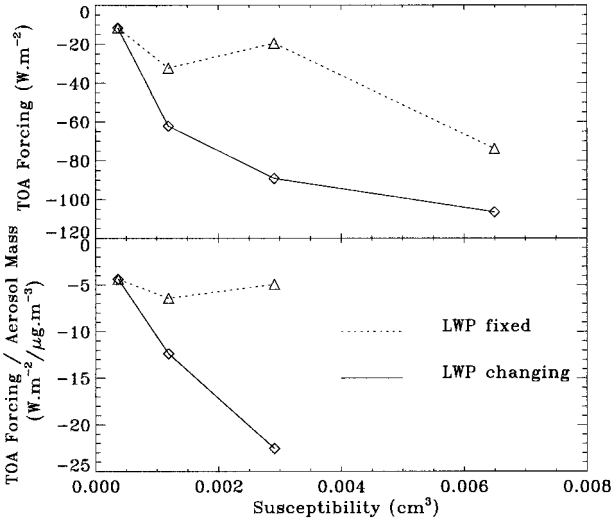

FIG. 5. (upper panel) Diurnally averaged top of atmosphere radiative forcing as a function of cloud susceptibility. (lower panel) As for upper panel but forcing is normalized by aerosol mass content assuming ammonium sulphate aerosol. In the lower panel the points for the high susceptibility are missing as the aerosol data were not available.

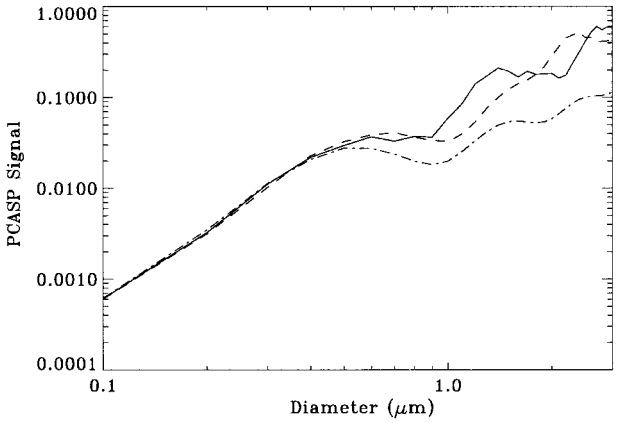

FIG. 6. The PCASP integrated angular response computed using Mie theory for water droplets (dashed line), ammonium sulphate (solid line), and carbon (dot-dashed line) as a function of droplet diameter.

lowed to change, the cloud was modeled by using the retrieved LWP and r_e. The r_e retrieved remotely, from measurements in the near-infrared, has been shown to be sensitive to all the droplets including the larger drizzle drops (Taylor and Ackerman 1999).

Aerosol concentrations in the accumulation mode (0.1–3.0-μm diameter) are measured using a PCASP by measuring the scattering of a laser beam by the aerosol. This sizing is carried out using a size-to-scatter relationship based on Mie theory for a water droplet. The chemistry of the aerosol is, however, variable and has refractive indices different from water. One can simulate the effects of different aerosol chemistry on the PCASP by carrying out Mie calculations for different refractive indices. The PCASP measures the scattered light over the collection range of 35°–120°. Figure 6 shows the PCASP integrated angular response computed using Mie theory for water droplets (dashed line), ammonium sulphate (solid line), and carbon (dot-dashed line) as a function of droplet diameter. As can be seen, the effects of the different aerosol compositions only become apparent for aerosol of $D > 0.4$ μm. Aerosol spectra, measured by the PCASP, from a transect through a ship plume on 29 June, flight A348, are shown in Fig. 7 for the background air, solid line, and the ship plume, dotted line. The difference between these two spectra is shown as triangles joined by a dashed line. A line at $D = 0.4$ μm has been added for reference. As can be seen from these spectra the increase in accumulation-mode aerosol measured by the PCASP is mainly within the $0.1 < D < 0.4$ μm region, a point supported by Hobbs et al. (2000), and hence the refractive indices of water used in the PCASP data processing are valid. The PCASP also dries the aerosol to some extent as it is gathered, and this is likely to change both the size and scattering properties of the aerosol before it passes through the laser beam. We are unable to quantify the exact amount of drying or its impact on these measurements but acknowledge this as a possible source of error in our calculations. It should be noted that the aerosol data for flight A346 came from a PMS ASASP-X optical particle counter since the PCASP was not operable during this flight. The ASASP-X has a similar response to the PCASP and is an integral part of an instrument used to measure the size spectra of aerosol that had been volatilized. The aerosol data from the ASASP-X were the concentrations counted before any of the aerosol was volatilized and hence was a measure of the ambient aerosol, as is the case for the PCASP.

The diurnally averaged top-of-atmosphere (TOA) forcing, R, for the four cases is shown in Fig. 5 as a

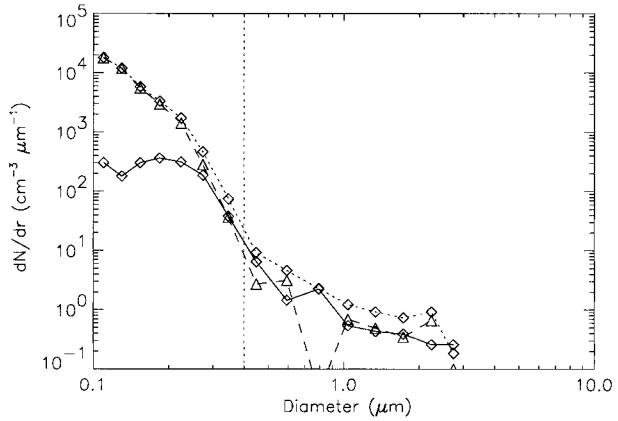

FIG. 7. Aerosol spectra, measured by the PCASP, from a transect through a ship plume on 29 Jun, flight A348, for the background air, solid line, and the ship plume, dotted line. The difference between these two spectra is shown as triangles joined by a dashed line. A line at $D = 0.4$ μm has been drawn for reference.

function of the background cloud susceptibility (upper panel). The diurnal average was modeled by assuming the background cloud and ship track cloud persisted in the same state as they were at the time of observation for an entire day. The effects of diurnal variation in cloud cover and microphysical properties were therefore ignored. In the marine boundary the relative effect of the increased aerosol on the cloud layer is likely to vary diurnally also. These results are meant to show the sensitivity of the cloud system to aerosol effects. The diurnal averaging used here is crude but returns numbers in a format that can be easily compared with general circulation models. In the lower panel the forcing R has been normalized by the aerosol mass content measured during a run just below cloud base. The indirect forcing of the first kind (size changes) is shown as a dashed line; the indirect forcing of the second kind (size and LWP changes) is shown as a solid line. The aerosol concentrations have been converted to a mass content by assuming the extra aerosol in the ship plume has the density of ammonium sulphate (1769 kg m^{-3}). Table 1 shows the aerosol and cloud microphysical properties for the four cases presented in Fig. 5. It should be noted that during flight A338, which corresponds to the point with the highest susceptibility in the upper panel, the cloud layer extended down to the surface and we were unable to fly below the cloud and measure the aerosol concentrations.

Using the data in the background cloud, for the cases where LWP changes and is fixed, it is possible to compute the additional fractional increase in the susceptibility caused by the variation in LWP, δ. This is equivalent to the term δ in the paper by Pincus and Baker (1994). For the last three cases given in Table 1, where there is variation in LWP, the values of delta are 2.31, 2.61, and 2.54, respectively. These values are consistent with those shown in Fig. 2 of Pincus and Baker (1994) where they show model simulations of δ as a function of droplet concentration.

As can be seen in the upper panel of Fig. 5 the diurnally averaged forcing can be very large for clouds of high susceptibility. The indirect aerosol forcing of the first kind, due to droplet size changes alone, is lower than the aerosol indirect forcing of the second kind, that due to the combined droplet size and LWP changes. The magnitude of the forcing is strongly dependent on the background LWP as well as the initial droplet size and varies substantially even within the same cloud field measured on the same day.

The pollution from a ship is concentrated over a relatively small volume and hence may be higher than would be expected from a more diffuse source such as a city. The normalized indirect aerosol forcings show considerable variation with cloud susceptibility with the largest forcings occurring for the most susceptible clouds. There is some evidence that an asymptote might be reached with clouds of high susceptibility, but more data is required to verify this. There appears to be a

TABLE 1. Boundary layer aerosol properties and microphysical properties of the background and ship track for the four cases modeled.

		Out of track					In track				
C-130 flight	Susceptibility (10^{-3} cm^3)	Aerosol concentration (cm^{-3})	Aerosol mass ($\mu g\ m^{-3}$)	Droplet concentration (cm^{-3})	Droplet r_e (μm)	LWP ($g\ m^{-2}$)	Aerosol concentration (cm^{-3})	Aerosol mass ($\mu g\ m^{-3}$)	Droplet concentration (cm^{-3})	Droplet r_e (μm)	LWP ($g\ m^{-2}$)
A346	0.368	511.2	4.87	92.8	8.3	45.5	667.1	6.36	135.7	7.3	45.5
A348**	1.188	64.3	4.47	27.4	13.8	124.7	282.2	7.23	71.7	6.9	188.8
A348**	2.911	64.9	9.51	23.9	15.1	161.2	1000.4	13.5	95.2	9.5	226.8
A338	6.495	*	*	12.2	19.4	71.2	*	*	59.6	9.2	100.7

* No boundary layer aerosol data available.
** LWP from microwave radiometer.

smaller variation when indirect forcing of the first kind only is considered, although it is acknowledged that the dataset is small. For the low-susceptibility case there was no observed change in liquid water content, and no drizzle was observed; hence the two forcing values are the same. For the higher-susceptibility cases the occurrence of changes in liquid water becomes increasingly more significant, increasing the forcing by up to a factor of 4.

Jones and Slingo (1996) modeled the impact of anthropogenic sulphates on clouds and computed global maps of annual mean forcing. The sulphate ion mass over the coast of California near Monterey, derived from the data of Langner and Rodhe (1991) (Jones, personal communication), is 0.65–0.67 μg m^{-3}. The TOA indirect forcing computed by Jones and Slingo varied depending on the parameterization used to relate aerosol amounts to changes in droplet size, but the annual mean forcing off the California coast varied from -1 to -4 W m^{-2}. These values, when normalized by Langner and Rodhe's sulphate ion mass contents, yield forcings with a range of values from -1.5 to -6.2 W m^{-2}/μg m^{-3}. These results are comparable in magnitude to the radiation modeling results presented in Fig. 5, bearing in mind that the modeling results of Jones and Slingo treat only indirect forcing of the first kind and hence can be compared only with the dashed lines in Fig. 5. It should also be noted that the Jones and Slingo results are annual averages, compared to the diurnal averages presented here. Also, the forcing computed for the ship track cases are those over a relatively small area with total cloud cover, as opposed to those of Jones and Slingo, which are regional estimates and will include variation in cloud fraction during the year. The data of Langner and Rodhe also refer to the total sulphate ion mass, whereas our results assume an ammonium sulphate aerosol.

It is informative to note that the Jones and Slingo results are broadly comparable with our results for indirect aerosol forcing of the first kind. However, our results suggest that an important process is not being represented in the GCM simulations and that the forcing could be even larger if indirect forcing of the second kind is considered (i.e., changes in LWP as a result of drizzle suppression combined with changes in droplet size). This increase in the TOA forcing may be important when considering climate studies resulting from anthropogenic aerosol emissions.

It should be noted that drizzle is sporadic in nature, and when averaged over an entire cloud field the effect of these regions of enhanced forcing will be reduced.

Drizzle occurrence and its relation to the TOA forcing

To determine the prevalence of drizzle in the marine boundary layer, and hence the possible importance of the enhanced forcing presented above, we have to turn to satellite data that provide greater spatial coverage.

Imagery from the *NOAA-12* advanced very high resolution radiometer (AVHRR) instruments has been analyzed to retrieve the cloud optical thickness and cloud-top effective radius using measurements in channels 1, 3, and 4. A thorough description of the retrieval scheme is given by Platnick and Valero (1995, hereafter PV95). Images from six days have been analyzed and the background cloud microphysical properties evaluated in the vicinity of ship tracks. The retrievals were carried out assuming a sea surface temperature of 287 K, which was derived from satellite measurements in clear skies and is in good agreement with aircraft measurements. The accuracy of the sea surface temperature and its effect on the observed thermal emission at 3.7 and 11 μm become increasingly important as the cloud optical thickness decreases. Also, for low cloud optical thicknesses, the possibility of spurious effective radius retrievals due to the presence of subpixel breaks in the cloud, increases. The effect of holes in the cloud is to increase the retrieved effective radius. In the analysis of the data presented here the effective radius data have been used only where the optical depth was greater than 5.

Using a different retrieval scheme (Coakley et al. 2000, hereafter C00), morning overpasses, *NOAA-12*, and afternoon overpasses, *NOAA-11*, were analyzed for the month of June 1994 to obtain optical depth and effective radius averaged over 60-km cloudy regions. This retrieval scheme showed systematic differences with droplet size being larger by 1–2 μm when compared with identical data used in the PV95 scheme; a full discussion of the differences is given in C00, but it is mainly attributable to the use of a double Henyey Greenstein phase function to approximate the higher moments of the Mie scattering phase function in the C00 scheme. Despite these differences, it is instructive to compare the predictions from these two schemes since they provide some insight into the absolute accuracy of the procedures. In the case of the C00 retrievals, measures were taken to ensure that the pixels used in the retrievals were overcast and the results did not show the pixels containing broken clouds or cloud holes. Nevertheless, to maintain compatibility with the PV95 results, optical depths were also restricted to be greater than 5 for the C00 retrievals. This data are for regions in the vicinity of ship tracks and for regions where no ship tracks were found.

Figure 8 shows a histogram of the frequency of occurrence of retrieved cloud optical depth using the PV95 scheme. The mean retrieved optical depth was 9.95 with a standard deviation of 3.78. The range of optical depths is large, from 3 to 24. Figure 9 shows a histogram of the frequency of occurrence of retrieved effective radius using the PV95 scheme (solid line) and the C00 scheme (dashed line). The PV95 data represent some 9000 individual groups of pixel retrievals in the unperturbed background cloud; approximately 4000 data points were neglected as the optical depth was less than or equal to 5. The C00 data represent 4014 60-km regions analyzed;

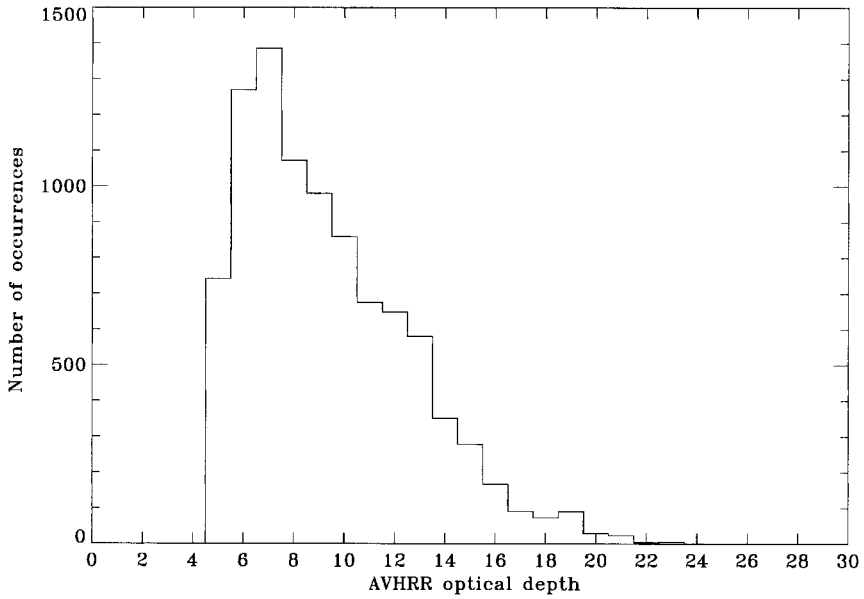

FIG. 8. Histogram of the frequency of occurrence of AVHRR retrieved cloud optical depth.

13 361 groups were neglected as the cloud optical depth was less than 5. As can be seen from this figure the range of effective radii retrieved is very large. It should be noted that beyond 20 μm the PV95 retrieval scheme has only a 2-μm resolution. It can be seen that the C00 scheme gives systematically larger r_e than the PV95 scheme, as discussed in Coakley et al. (2000).

Han et al. (1995) used ground-based microwave radiometer and ceilometer data to determine the presence of drizzle over San Nicolas Island during FIRE 87. They then compared the occurrence of drizzle episodes with effective radii retrieved from the ISCCP satellite data. Han et al. suggested that clouds with effective radii greater than 15 μm appeared to be associated with drizzle episodes, whereas those with effective radii less than 10 μm did not.

Figure 10 shows the percentage of cases where the AVHRR retrieved r_e exceeds some threshold r_e plotted on the abscissa. The diamonds are results from six days of *NOAA-12* imagery processed with the PV95 scheme;

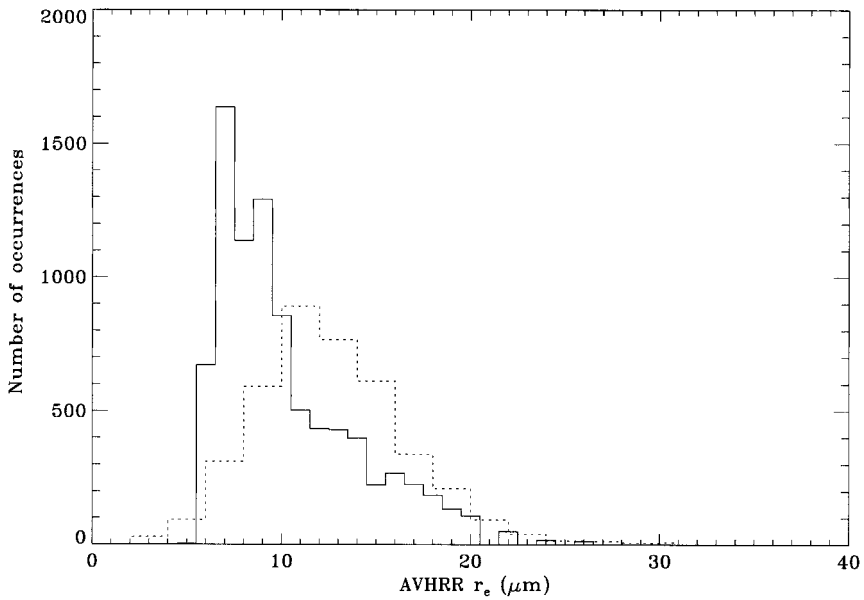

FIG. 9. Histogram of the frequency of occurrence of AVHRR retrieved cloud-top effective radius, using the PV95 scheme, solid line, and the C00 scheme, dashed line.

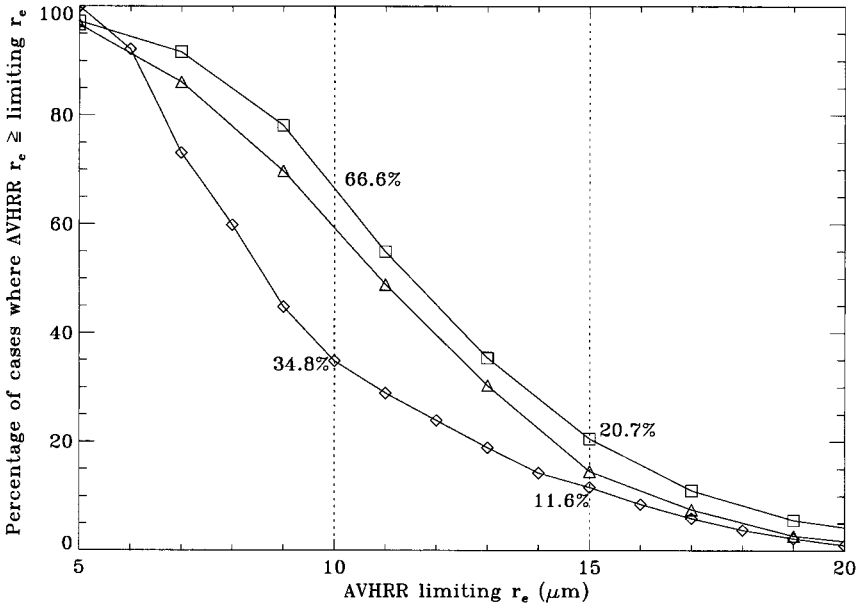

FIG. 10. The percentage of pixel groups with effective radius greater than some limiting effective radius. Diamonds are results from the PV95 scheme; triangles those from morning overpasses using the C00 scheme; and squares are the afternoon overpasses using the C00 scheme.

the triangles are for the *NOAA-12* morning overpasses processed using the C00 scheme; and the squares are for the *NOAA-11* afternoon overpasses again processed using the C00 scheme. If we use the Han et al. criteria for the presence of drizzle we see that between 34.8% and 66.6% of the pixel groups had an r_e of > 10 μm and between 11.6% and 20.7% had an $r_e > 15$ μm. There is an obvious difference between the two retrieval schemes for $r_e < 15$ μm, which is probably due to the systematic differences described earlier. These results suggest that the occurrence of drizzle drops in marine stratocumulus is not uncommon. It should not be assumed that drizzle occurs in all clouds where $r_e > 15$ μm; further work is required to study the occurrence and distribution of drizzle. The satellite imagery analyzed using the PV95 scheme is that from cloud in which ship tracks were formed, although the data are of the unperturbed background cloud. Therefore, there is a bias in this sample since ship tracks are observed only in relatively clean air masses and these air masses would be expected to have more drizzle than a continental air mass. The percentage occurrence of drizzle ascertained from this imagery may be too high if it is used as an estimate of the global occurrence, although it is not possible to say by what amount. The imagery analyzed using the C00 scheme, however, is for all cloud regions. It is shown in C00 that there is little difference in the distribution of r_e between clouds within 200 km of ship tracks and those outside that region. It is therefore reasonable to assume that our results are representative of the variability observed off the Californian coast.

Han et al. (1994) present a near-global survey of r_e retrieved from ISCCP satellite data. Their data are therefore from a wide range of air masses, both of maritime and continental influence. Their histograms of the percentage occurrence of cloud-top r_e in various latitude bands suggest that there is around a 10%–15% occurrence of r_e greater than 15 μm. These figures would suggest that the MAST analyses do represent a reasonable representation of the global occurrence of drizzle.

Combining these two datasets one could postulate that drizzle occurs in some 10% of marine boundary layer clouds. This analysis has been based on the assumption that the occurrence of drizzle can be identified on the basis of cloud-top r_e alone. This is unlikely to be the case, and other features such as cloud thickness and liquid water content are also likely to be of importance. Also drizzle is sporadic in nature and is likely to exhibit large temporal variability.

6. Discussion and conclusions

We have shown that the clouds observed during the MAST campaign are very variable in their susceptibility and that this susceptibility can be used as an indicator of the sensitivity of the clouds to modification by anthropogenic pollution. Ship tracks have proven useful as a means of studying these processes in a confined region and have provided some quantitative measure of the possible magnitudes of these effects. Ship tracks themselves are not significant on climate scales because of their limited spatial extent. However, they do provide measurable examples of albedo modification that can aid understanding of the impact of aerosols on cloud radiative properties. It is important to note, however, that pollution on a larger scale, from say a city or con-

tinent, is likely to take place over a longer timescale, and hence the variability in the natural life cycles of clouds will play a more significant role. Also, the ship track phenomenon represents pollution in a relatively small area surrounded by clean clouds, and there will be interactions across the boundaries of these two air masses that may not occur on the larger scale.

The data presented here clearly show that the TOA forcing resulting from anthropogenic aerosol emissions can be substantial and that the magnitude of this TOA forcing can be significantly enhanced if cloud liquid water path is modified in addition to changes to the cloud droplet size. Changes in LWP will occur only if drizzle suppression is induced as a result of the reduced droplet size in the polluted cloud. Our results show that the magnitude of the changes in LWP and r_e are strongly dependant on the susceptibility of the background cloud.

The magnitude of the changes in TOA forcing presented here are large and possibly significant on a climate level, but they will only be of significance on a global level if drizzle is prevalent in the marine atmosphere. Our results of limited AVHRR analysis suggest that the occurrence of marine clouds that support drizzle may be of the order of 10%. Further information on the lifetime and distribution of drizzle is not currently available in the literature. It should be noted that the drizzle cells encountered in the aircraft transects are instantaneous measurements that have then been used to compute diurnal average TOA forcing. In reality such a drizzle cell, and hence such a change in LWP relative to the background, is not likely to persist all day. Drizzle is sporadic in nature, and its lifetime is not known but is unlikely to be more than a few hours.

Many factors may act to decrease the magnitude of the TOA forcing resulting from changes in cloud LWP induced by increases in aerosol concentration. The lifetime of drizzle, the possible variation in drizzle with the overlying diurnal variation in cloud cover, and the percentage occurrence of drizzle are just a few possibilities that can act to reduce the impact of this forcing on climate. The actual magnitude of these impacts can be estimated only by modeling the full cycle of a stratocumulus sheet. However, the results presented here do highlight the maximum magnitude of these effects and show that this is a potentially important process worthy of further study.

An analysis of AVHRR imagery by Platnick et al. (2000) has shown that not all ship tracks can be related to an increase in LWP. In fact, their results suggest there was a slight decrease in LWP when averaged over all tracks, though the change was highly variable for any given track location. The highly variable nature of the background cloud is obviously a problem in such analysis, but it is clear that the relationship between aerosols and cloud LWP is not straightforward and warrants further study.

Acknowledgments. We would like to thank the MRF scientists and Royal Air Force aircrew of the MRF C-130 and the C-131A aircrew for their efforts in obtaining the data used in this paper. The coordination of the MAST experiment was carried out by Phil Durkee and Bob Bluth, and their contribution is greatly appreciated.

REFERENCES

Albrecht, B. A., 1989: Aerosols, cloud microphysics and fractional cloudiness. *Science,* **245,** 1227–1230.

Braham, R. R., Jr., 1974: Cloud physics of urban weather modification—A preliminary report. *Bull. Amer. Meteor. Soc.,* **55,** 100–106.

Brown, P. R. A., 1993: Measurements of the ice water content in cirrus using an evaporative technique. *J. Atmos. Oceanic Technol.,* **10,** 579–590.

Charlson, R. J., S. E. Schwartz, J. M. Hales, R. D. Cess, J. A. Coakley, J. E. Hansen, and D. J. Hofman, 1992: Climate forcing by anthropogenic aerosols. *Science,* **255,** 423–430.

Coakley, J. A., Jr., R. L. Bernstein, and P. A. Durkee, 1987: Effect of ship track effluents on cloud reflectivity. *Science,* **237,** 1020–1022.

——, and Coauthors, 2000: The appearance and disappearance of ship tracks on large spatial scales. *J. Atmos. Sci.,* **57,** 2765–2778.

Conover, J. H., 1966: Anomalous cloud lines. *J. Atmos. Sci.,* **23,** 778–785.

Durkee, P. A., K. J. Noone, and R. T. Bluth, 2000: The Monterey Area Ship Track experiment. *J. Atmos. Sci.,* **57,** 2523–2541.

Eagan, R. C., P. V. Hobbs, and L. F. Radke, 1974: Particle emissions from a large Kraft paper mill and their effects on the microstructure of warm clouds. *J. Appl. Meteor.,* **13,** 535–552.

Edwards, J. M., and A. Slingo, 1996: Studies with a flexible new radiation code. I: Choosing a configuration for a large scale model. *Quart. J. Roy. Meteor. Soc.,* **122,** 689–719.

English, S. J., 1995: Airborne radiometric observations of cloud liquid-water emission at 89 and 157 GHz: Application to retrieval of liquid-water path. *Quart. J. Roy. Meteor. Soc.,* **121,** 1501–1524.

——, C. Guillou, C. Prigent, and D. C. Jones, 1994: Aircraft measurements of water vapour continuum absorption at millimetre wavelengths. *Quart. J. Roy. Meteor. Soc.,* **120,** 603–625.

Ferek, R. J., D. A. Hegg, P. V. Hobbs, P. A. Durkee, and K. Nielsen, 1998: Measurements of ship-induced tracks in clouds off the Washington coast. *J. Geophys. Res.,* **103,** 23 199–23 206.

——, and Coauthors, 2000: Drizzle suppression in ship tracks. *J. Atmos. Sci.,* **57,** 2707–2728.

Goody, R. M., and Y. L. Yung, 1989: *Atmospheric Radiation.* 2d ed. Oxford University Press, 519 pp.

Han, Q., W. Rossow, and A. A. Lacis, 1994: Near-global survey of effective droplet radii in liquid water clouds using ISCCP data. *J. Climate,* **7,** 465–497.

——, ——, R. Welch, A. White, and J. Chou, 1995: Validation of satellite retrievals of cloud microphysics and liquid water path using observations from FIRE. *J. Atmos. Sci.,* **52,** 4183–4195.

Hobbs, P. V., 1993: Aerosol–cloud interactions. *Aerosol–Cloud–Climate Interactions,* P. V. Hobbs, Ed., Academic Press, 33–73.

——, L. F. Radke, and S. E. Shumway, 1970: Cloud condensation nuclei from industrial sources and their apparent influence on precipitation in Washington State. *J. Atmos. Sci.,* **27,** 81–89.

——, H. Harrison, and E. Robinson, 1974: Atmospheric effects of pollutants. *Science,* **183,** 909–915.

——, L. F. Radke, J. H. Lyons, R. J. Ferek, D. J. Coffman, and T. J. Casadevall, 1991: Airborne measurements of particle and gas emissions from the 1990 volcanic eruptions of Mt. Redoubt. *J. Geophys. Res.,* **96,** 18 735–18 752.

——, and Coauthors, 2000: Emissions from ships with respect to their effects on clouds. *J. Atmos. Sci.,* **57,** 2570–2590.

Houghton, J. T., G. J. Jenkins, and J. J. Ephraums, Eds., 1990: *Climate Change. The IPCC Scientific Assessment.* Cambridge University Press, 365 pp.

Jones, A., and A. Slingo, 1996: Predicting cloud droplet effective radius and indirect sulphate aerosol forcing using a general circulation model. *Quart. J. Roy. Meteor. Soc.,* **122,** 1573–1595.

Jones, D. C., 1991: Microwave Airborne Radiometer Scanning System: Calibration and initial performance assessment. Met O(RSI) Branch Memo. 3. [Available from National Meteorological Library, London Road, Bracknell, Berkshire, RG12 2SZ, United Kingdom.]

Kilsby, C. G., D. P. Edwards, R. W. Saunders, and J. S. Foot, 1992: Water-vapour continuum absorption in the tropics: Aircraft measurements and model comparisons. *Quart. J. Roy. Meteor. Soc.*, **118,** 715–748.

Langner, J., and H. Rodhe, 1991: A global three-dimensional model of the tropospheric sulfur cycle. *J. Atmos. Chem.,* **13,** 225–263.

Martin, G. M., D. W. Johnson, and A. Spice, 1994: The measurement and parametrisation of the effective radius of warm stratocumulus clouds. *J. Atmos. Sci.,* **51,** 1823–1842.

McClatchey, R. A., R. W. Fenn, J. E. A. Selby, F. E. Volz, and J. S. Garing, 1972: Optical properties of the atmosphere. 3d ed. Air Force Cambridge Research Laboratories, 108 pp.

Pincus, R., and M. B. Baker, 1994: Effect of precipitation on the albedo susceptibility of clouds in the marine boundary layer. *Nature,* **372,** 250–252.

Platnick, S., and S. Twomey, 1994: Determining the susceptibility of cloud albedo to changes in drop concentration with the Advanced Very High Resolution Radiometer. *J. Appl. Meteor.,* **33,** 334–347.

——, and F. P. J. Valero, 1995: A validation of a satellite cloud retrieval during ASTEX. *J. Atmos. Sci.,* **52,** 2985–3001.

——, and Coauthors, 2000: The role of background cloud microphysics in the radiative formation of ship tracks. *J. Atmos. Sci.*, **57,** 2607–2624.

Radke, L. F., J. A. Coakley, and M. D. King, 1989: Direct and remote sensing observations of the effects of ships on clouds. *Science,* **246,** 1146–1149.

Rawlins, F., and J. S. Foot, 1990: Remotely sensed measurements of stratocumulus properties during FIRE using the C-130 aircraft multichannel radiometer. *J. Atmos. Sci.,* **47,** 2488–2503.

Rogers, D. P., D. W. Johnson, and C. A. Friehe, 1995: The stable internal boundary layer over a coastal sea. Part 1: Airborne measurements of the mean turbulence structure. *J. Atmos. Sci.,* **52,** 667–683.

Saunders, R. W., G. Brogniez, J. C. Buriez, R. Meerkötter, and P. Wendling, 1992: A comparison of measured and modeled broadband fluxes from aircraft data during the ICE '89 field experiment. *J. Atmos. Oceanic Technol.,* **9,** 391–406.

Slingo, A., and H. M. Schrecker, 1982: On the shortwave radiative properties of stratiform water clouds. *Quart. J. Roy. Meteor. Soc.,* **108,** 407–426.

Squires, P., and S. Twomey, 1960: The relation between cloud droplet spectra and the spectrum of cloud nuclei. *Physics of Precipitation, Geophys. Monogr.,* No. 5, Amer. Geophys. Union, 211–219.

Taylor, J. P., 1992: Sensitivity of remotely sensed effective radius of cloud droplets to changes in LOWTRAN version. *J. Atmos. Sci.*, **49,** 2564–2569.

——, 1994: Measurements of the radiative and microphysical properties of stratocumulus over the South Atlantic and around the British Isles. *Atmos. Res.,* **34,** 27–41.

——, and A. McHaffie, 1994: Measurements of cloud susceptibility. *J. Atmos. Sci.,* **51,** 1298–1306.

——, and S. J. English, 1995: The retrieval of cloud radiative and microphysical properties using combined near-infrared and microwave radiometry. *Quart. J. Roy. Meteor. Soc.,* **121,** 1083–1112.

——, and A. S. Ackerman, 1999: A case-study of pronounced perturbations to cloud properties and boundary-layer dynamics due to aerosol emissions. *Quart. J. Roy. Meteor. Soc.,* **125,** 2643–2661.

——, J. M. Edwards, M. D. Glew, P. Hignett, and A. Slingo, 1996: Studies with a flexible new radiation code. II: Comparisons with aircraft shortwave observations. *Quart. J. Roy. Meteor. Soc.,* **122,** 839–861.

Twomey, S., 1974: Pollution and planetary albedo. *Atmos. Environ.,* **8,** 1251–1256.

——, 1977: The influence of pollution on the shortwave albedo of clouds. *J. Atmos. Sci.,* **34,** 1149–1152.

——, M. Piepgrass, and T. L. Wolfe, 1984: An assessment of the impact of pollution on global cloud albedo. *Tellus,* **36B,** 356–366.